Investigation into the effect of asymmetric train speed distribution on rail corrugation growth in cornering

R.D. Batten, P.A. Bellette and P.A. Meehan

Rail CRC, School of Engineering, University of Queensland, Brisbane, QLD 4072, Australia

ABSTRACT

The transportation phenomenon known as wear-type rail corrugation is a significant problem in railway engineering, manifesting as an oscillatory wear pattern on the rail head. These profile variations induce unwanted vibrations, excessive noise and other associated problems. Recent studies have shown that uniformity in train passing speed accelerates the corrugation growth process and conversely, widening the probabilistic speed distribution can be used as a mitigation tool. This paper investigates the effects of an asymmetric speed distribution on corrugation growth rate for a train in cornering. A frequency domain corrugation growth prediction model, based on experimental vertical rail receptance, is developed further to achieve this. Results provide insight into optimum asymmetric conditions required to minimize corrugation growth using speed distribution control.

INTRODUCTION

Wear-type rail corrugation is a periodic wear pattern developing on running rail heads with extended use. It has a characteristic wavelength of 25-400mm and is a significant problem in the railway transport industries worldwide (Sato, 2002). This surface irregularity grows exponentially as a function of train passages often causing serious unwanted noise and vibration. Figure 1 shows a corrugation profile observed in the field after approximately 9 months of passenger rail traffic.

Figure 1. 9 month old corrugated rail profile

Wear-type rail corrugation is caused by oscillatory contact conditions between the wheel and rail, resulting in a variance in frictional power between the two running surfaces. This in turn wears the surface of the rail periodically, resulting in a vertical ripple pattern on the rail head. The resultant profile variance then accelerates this process on subsequent wheel passages, growing the amplitude of corrugation exponentially with additional train passes (see Hempelmann, 1991).

The oscillating contact conditions associated with a corrugated section of rail can cause excessive noise and structural vibrations in the train and track, inevitably requiring a complete reprofiling of the track with use of a rail grinder. Currently in Australia, this process is costing the rail industry in excess of AU$ 10 million every year and will continue to become more costly with predicted increases in rail traffic density unless alternative mitigation methods are put in place.

Recent studies have shown that uniformity in train passing speed facilitates rapid corrugation growth and that widening the probabilistic passing speed distribution on a given section of rail can be used as an effective mitigation tool (Bellette, 2008 and Hoffman and Misol, 2007). Often though, the variance of train speed approved by rail operators will be limited in order to maintain existing timetables. For this reason, additional increase of train passing speed standard deviation may not be possible so alternative methods of speed control based corrugation growth control may be necessary.

This paper adds to a previously developed frequency domain corrugation prediction model to predict and quantify the effects of using an asymmetric speed distribution curve on the overall corrugation growth rate. In particular, optimal asymmetric parameters are determined and the additional benefit of asymmetry in corrugation control under a range of parameters is determined.

THEORETICAL MODELLING

The model used in this paper is based on a previously developed frequency domain dynamic normal force (Bellette, 2008). Previous to this paper the model assumed constant steady state growth parameters with speed. In the presence of a wider speed distribution, any effects due to an asymmetric speed distribution on the expected growth rate were inconsequential. With a fixed average and standard deviation of speed however, these effects must be considered.

The following subsections outline the modelling techniques used to evaluate the two main components of the growth equation. These components are: the dynamic normal force function with frequency and the growth multiplier made up of the steady state wear, normal force and creep sensitivity, all functions of passing speed.

Wear sensitivity to contact deflection

The wear sensitivity, K_b, refers to the term in the frequency domain transfer function made up of the product of steady

state cornering parameters of wear depth, Δz_0, low rail normal force, P_L, contact stiffness, k_c, and creep sensitivity, $C_{\xi P}$. Equation 1 shows this term explicitly (Bellette, 2008).

$$K_b = \frac{\Delta z_0 C_{\xi P} k_c}{P_L} \tag{1}$$

First stage in evaluating the wear sensitivity for the dynamic normal force function is to find the steady state cornering normal forces on the high and low rails. This was done via force balance calculations to find the steady state wagon roll and subsequently the vertical reaction forces through the rails.

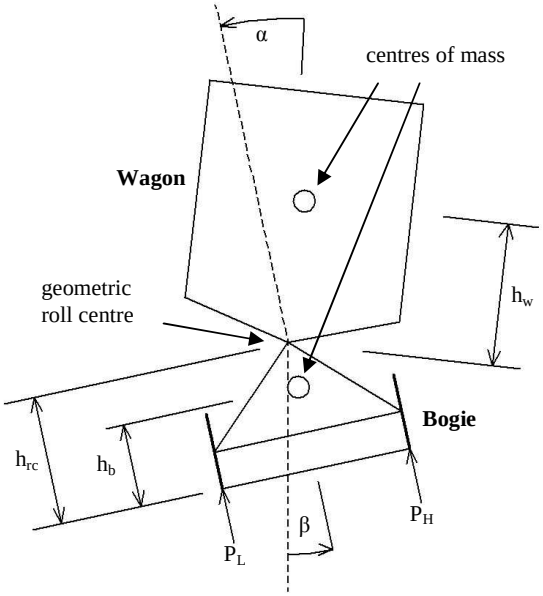

Figure 2. Wagon roll, rail reaction forces and associated train parameters

Equation 2 shows the wagon roll angle reached in steady state cornering. This is calculated via moment balance of forces above the wagon roll centre about the geometric roll centre defined by the suspension setup.

$$\alpha(v) = \frac{g \cdot h_w \cdot \beta - v^2 / r \cdot h_w}{g \cdot h_w - k_{roll} / m_w} \tag{2}$$

With the cornering wagon roll defined the normal forces on the high and low rails can be calculated via global moment balance about the opposing rails. Equations 3 and 4 take inputs of wagon and bogie properties and return a steady state normal force on the high and low rails respectively.

$$P_L = \left(\frac{(m_w h_{rc} + m_b h_b) g}{w} + \frac{m v^2}{2r} \right) \sin(\beta) + \left(\frac{mg}{2} - \frac{(m_w h_{rc} + m_b h_b) v^2}{rw} \right) \cos(\beta) - \frac{k_{roll} \alpha}{w} \tag{3}$$

$$P_H = \left(\frac{m v^2}{2r} - \frac{(m_w h_{rc} + m_b h_b) g}{G} \right) \sin(\beta) + \left(\frac{mg}{2} + \frac{(m_w h_{rc} + m_b h_b) v^2}{rG} \right) \cos(\beta) + \frac{k_{roll} \alpha}{G} \tag{4}$$

In order to evaluate the growth multiplier for a given speed, the steady state cornering position of the bogie must be calculated. This was achieved by numerical optimization of total traction forces on the bogie to cancel the cornering radial acceleration.

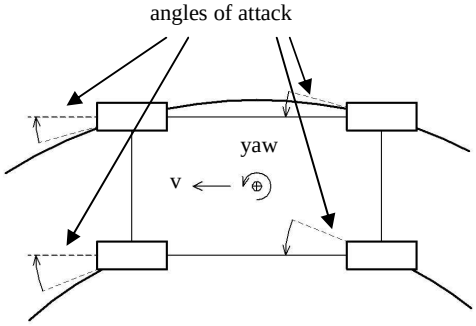

Figure 3. Wheel angles of attack at zero bogie yaw

The traction forces were calculated based on a predicted bogie yaw used to find angles of attack of each of the four wheels. The angle of attack is the geometrically constrained angle of attack at zero yaw, offset by the given yaw angle. With angles of attack and tangential velocity of the train known, the slip ratios on each wheel could be calculated.

$$\theta_i = \arcsin(L / (2r_i)) \tag{5}$$

$$w_i = \sin(\theta_i + y) \tag{6}$$

It was assumed that the longitudinal slip and traction is negligible compared to lateral, allowing the traction ratio, μ_i, to be calculated based on a combination of work from using the model of Shen (1993) and Polach (2003) with a small modification to the friction coefficient exponent to constrain the peak traction ratio position (Daniel 2006). The equations are an empirical curve fit to experimental data for traction ratio variance with slip ratio, w_i, normalized to a critical slip ratio, w_c.

$$\mu_i = \mu_0 \left[\left(1 - \frac{\mu_0}{\mu_\infty} \right) e^{-B\left(\frac{w_i}{w_c} - 1 \right)} + \frac{\mu_0}{\mu_\infty} \right] \tag{7}$$

For w < 1, $$Q_i = \mu_i P_i \left(1 - \left(1 - \frac{w_i}{w_c} \right)^3 \right) \tag{8}$$

For w ≤ 1, $$Q_i = \mu_i P_i \tag{9}$$

Steady state cornering conditions are reached when the sum of lateral tractions balances the centripetal and gravitational force components in the direction perpendicular to the normal of the rails. A numerical optimization routine was used to find the steady state bogie yaw and subsequently all contact conditions for each given speed.

The steady state wear is a function of frictional power, train velocity, the half width of the contact patch, *b*, the material density of the rail, ρ, and an experimental wear coefficient, k_0 (see Kampfer, 2006), explicitly given by,

$$\Delta z_0 = \frac{k_0 P_L \mu w}{2b\rho} \tag{10}$$

The creep sensitivity is determined by calculating the differential of the creep curve for each set of cornering conditions. At creep ratios below critical, this differential is given by equation 11. Above critical slip, a numerical differential was preferred.

$$C_{\xi P} = \frac{2 - w/w_c}{3 - \left(1 - w/w_c\right)^2} \tag{11}$$

Dynamic normal force with speed variance

Corrugation forms due to the presence of oscillating frictional power which in turn is a function of slip ratio and normal force. For this reason, corrugation growth is maximized at frequencies where normal forcing and slip variation is maximized.

In the presence of large lateral damping due to the contact mechanics below critical slip (above critical the damping forces are negative), the slip variation on a corrugated profile becomes dependent on purely the vertical receptances of the track and wheel (see Meehan *et. al.*, 2009). A high track receptance will absorb the energy produced by an existing corrugated profile while a high negative wheel receptance will accentuate it.

It has been previously shown (see Grassie, 1984) that the transfer function between dynamic normal force and an existing corrugation profile is given by

$$\frac{\Delta P}{k_c Z_n(\omega)} = \frac{1}{1 + k_c \left(R_{rv}(\omega) + R_{wv}(\omega)\right)}, \tag{12}$$

where R_{rv} and R_{wv} are the vertical rail and wheel receptance functions and k_c is the contact stiffness, predetermined by the steady state normal force, (Johnson, 1987). This can be then be used to create a growth rate function for successive wheel set passes.

$$\frac{Z_{n+1}}{Z_n} = K_b \frac{\Delta P}{k_c Z_n(\omega)} + 1 \tag{13}$$

It's important to consider here that conditions alternate between each successive wheel set pass as every bogie will have a leading and trailing wheel set under different steady state cornering condition. A growth rate for a single equivalent wheel pass may be calculated based on an averaging of a full bogie pass.

$$\frac{Z_{n+1}}{Z_n} = \sqrt{\frac{Z_{n+2}}{Z_n}} = K_{b/eq} \frac{\Delta P}{k_c Z_n(\omega)} + 1 \tag{14}$$

At growth rates much less than one, the equivalent wear sensitivity is simply the average of those of the leading and trailing wheel set of the bogie.

$$K_{b/eq} = \frac{\left(K_{b(n\to n+1)} + K_{b(n+1\to n+2)}\right)}{2} \tag{15}$$

When a probabilistic speed distribution, p(x) is introduced (Meehan *et. al.*, 2009), the growth rate function then becomes

$$\frac{Z_{n+1}}{Z_n} = \exp \int_{-\infty}^{\infty} \ln \left| K_{b/eq} \frac{\Delta P}{k_c Z_n(\omega)} + 1 \right| \mathrm{p(x)} dx \tag{16}$$

The growth rate is a function of spatial frequency of corrugation. Therefore growth rate of the dominant wavelength of corrugation will be the maximum of this function with spatial frequency.

PROBABILISTIC PASSING SPEED

In order to investigate the effects of speed distribution asymmetry on growth rate, a triangular probability density function was used. Two constraint cases were defined as being constant average, constant standard deviation, and constant average, constant domain width. Limits of mode were chosen as full right angled left and right skewed curves and domain extremes were calculated to maintain the defined constraint cases. Figure 4 shows a generic triangular skewed distribution curve with labels of domain limits, mode and maximum height.

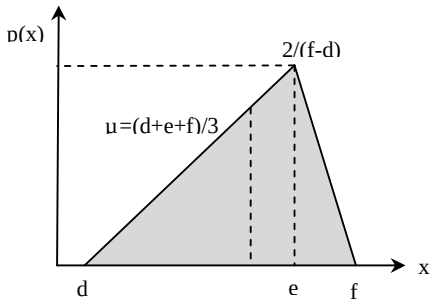

Figure 4. Skewed triangular speed distribution curve used in simulation

Equations 17 and 18 show the equations of domain limits for each chosen mode based on the predetermined average, $\overline{x}$ and standard deviation, σ.

$$d = \frac{3\overline{x} - e}{2} - \frac{\sqrt{-3e^2 + 6\overline{x} \cdot e - 3\overline{x}^2 + 24\sigma^2)}}{2} \tag{17}$$

$$f = \frac{3\overline{x} - e}{2} + \frac{\sqrt{-3e^2 + 6\overline{x} \cdot e - 3\overline{x}^2 + 24\sigma^2)}}{2} \tag{18}$$

Equations 19 and 20 show the equations of domain limits for a given mode based on predetermined average speed and domain width, *W*.

$$d = \frac{3\overline{x} - e}{2} - W/2 \tag{19}$$

$$f = \frac{3\overline{x} - e}{2} + W/2 \tag{20}$$

25 different evenly spaced modes were chosen between its limits and 100 speeds were integrated within the domain of each associated distribution curve. Figure 5 shows the com-

plete series of speed distribution curves with dashed and dotted lines of mean and one standard deviation respective marked for fixed standard deviation and Figure 6 shows the same but for fixed domain width.

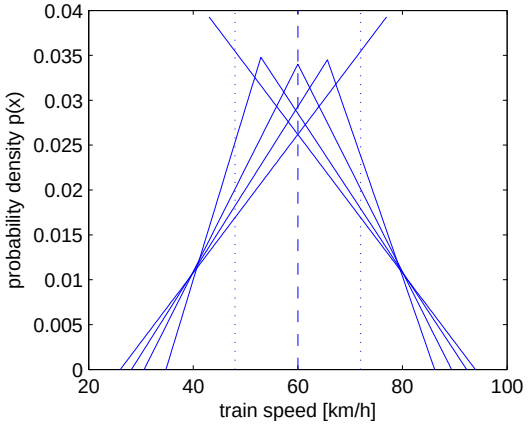

Figure 5. Simulated fixed standard deviation speed distribution curves with marked average (- - -) and standard deviation (. . .)

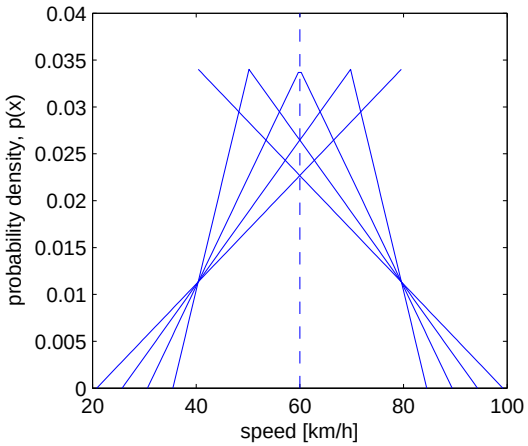

Figure 6. Simulated fixed domain width speed distribution curves with marked average (---)

SIMULATION RESULTS

Simulation parameters were chosen to represent a generic site by typical Brisbane suburban standards (see Appendix B). A 5 mode track model was introduced to model the vertical track receptance (see Appendix C) and the wheel receptance was assumed to be that of the unsprung Newtonian mass. The growth rate function was integrated numerically with each given speed distribution shape as a function of corrugation wavelength. The maximums in the frequency domain were then used to evaluate the dominant growth rate.

Figures 7 and 8 show the growth rate plotted against wavelength for fixed standard deviation and fixed domain width in speed and figure 9 shows the maximum growth rate against standard skewness, S, for both constraint conditions. Note that a negative skewness indicates skew towards high speed and a positive skewness to low speed.

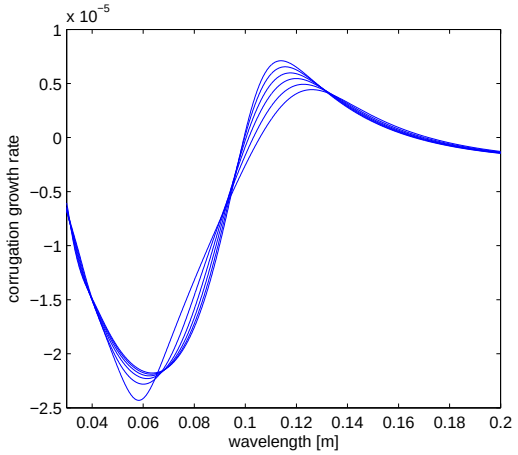

Figure 7. Corrugation growth rate as a function of wavelength for all tested fixed standard deviation distribution curves

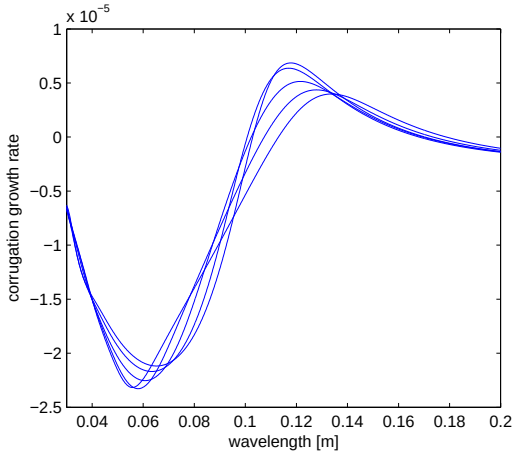

Figure 8. Corrugation growth rate as a function of wavelength for all tested fixed domain width distribution curves

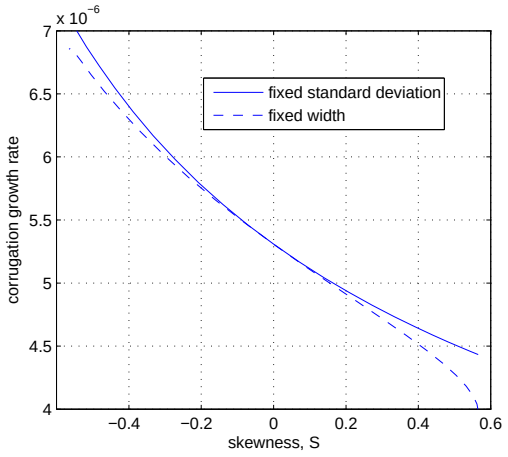

Figure 9. Corrugation growth rate change with standard skewness

Under the given parameters the growth rate can vary by up to 34% from that of a symmetric distribution. The trend is towards higher corrugation growth rate with speed distributions skewed towards higher speed.

It was also desired to test the integral of the dynamic normal force with fixed wear sensitivity and trends in wear sensitivity with speed to determine where trends in the growth rate with skew stem from. Figures 10 and 11 show the maximum growth rate at fixed wear sensitivity with skewness and wear sensitivity variance with train speed respectively.

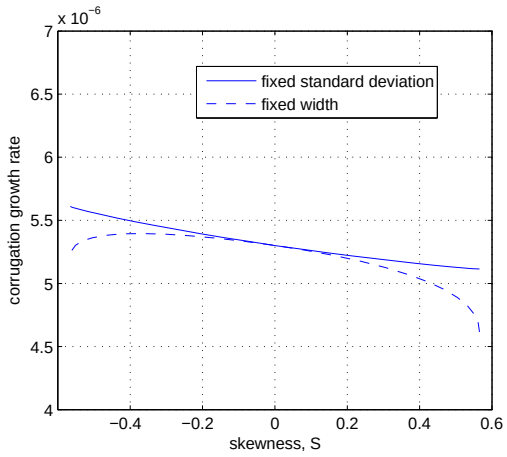

Figure 10. Corrugation growth rate for all distribution shapes with fixed wear sensitivity

It's clear that a trend in the dynamic normal force is present although less evident, even with the absence of variance in wear sensitivity with speed. The same apparent desensitivity to skewness will likely also occur with reducing the standard deviation of the curves.

The higher growth rate correlates to a slightly lower wavelength as seen in figures 7 and 8, opposite to what would be expected if the speeds to which the distribution curve was skewed were those at which corrugation growth was most readily occurring.

It has been shown that corrugation control via speed control correlates to increasing the damping on the corrugation forming peaks, lowering the dominant frequency along with the peak spectral density. This is likely the effect seen here.

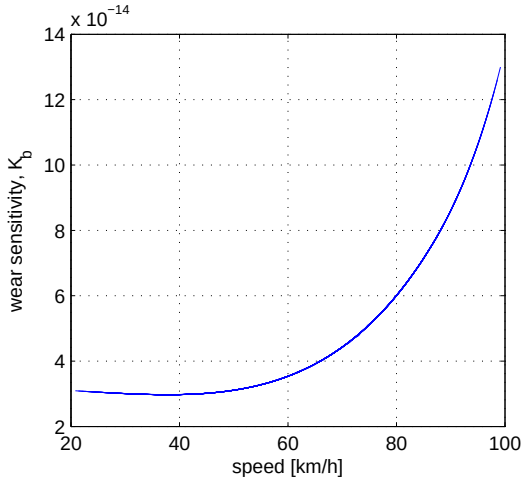

Figure 11. Wear sensitivity change with train speed

The wear sensitivity function shows local minima where the track cant angle neutralizes the centripetal force experienced by the cornering train. Typically tracks will be under-canted for a given site for the expected average train passing speed. For this reason, lateral loading of the wheels at their contact points and subsequently the steady state wear and inverse of normal force will increase with train speed from nominal conditions.

DISCUSSION

Speed distribution asymmetry was shown to potentially have a substantial effect on the maximum growth rate of corrugation. Given a constant average train speed with fixed standard deviation the growth rate could be reduced by up to 17% from that of a symmetric speed distribution curve under the given site parameters. Similar results were found with fixed speed range. This minimum occurred at low speed skew while a high speed skew showed a potential increase in growth rate of 34%. This means that under certain site conditions speed control without modification of the average or standard deviation in passing speed is viable.

The observed trend in maximum growth rate with speed distribution skew was the result of two compounding effects. The first is an increase in corrugation growth at the dominant wavelength due to widening of the spectral density peaks in the spatial frequency domain with increased speed. Given a fixed peak width in the time-based frequency domain, increasing the passing speed widens in the spatial domain with

$$\text{wavelength range} = \frac{\text{velocity}}{\text{frequency range}}.$$

The range of speed that promotes growth to the dominant wavelength remains constant as a percentage of the nominal. This means that for a given wavelength of corrugation, a greater range of speeds will result in significant growth at that particular wavelength if there is a skew towards higher speeds in that range, resulting in higher overall growth.

This effect was shown to occur even when the wear sensitivity remains constant. The second effect is that of an increase in the wear sensitivity function with increasing speed when the track is under-canted, resulting in increased growth across all frequencies with distributions shapes that show higher density at higher than average speeds.

Often a rail operator will prescribe a maximum or minimum speed on a given section of rail. This will often require skewing the speed distribution curve to maintain a chosen average if corrugation control via speed variance increase is used. If a lower limit of train speed is dictated the widest standard deviation is obtained for a given average when the speed distribution is skewed towards lower speed. Conversely, when an upper speed limit is enforced, a distribution curve skewed towards high speed will result in the widest variance.

This presents a problem in that the work presented in this paper shows that skewing the distribution curve in this manner can cause a significant increase in rail corrugation growth. For this reason, the effects of having a potentially skewed speed distribution curve should be considered before corrugation control via speed variance increase is used at a chosen site.

CONCLUSIONS

An existing frequency domain corrugation growth model was modified to investigate the effects of an asymmetric speed distribution curve on the maximum growth rate. Results showed that maximum corrugation growth rate changed significantly in the presence of an asymmetric speed distribution. Under typical site parameters a skew in the distribution

curve toward low speed caused a decrease in corrugation growth while higher speed skew caused an increase.

Under the given site parameters a 17% reduction in corrugation growth rate from that of a symmetric triangular distribution could be achieved by skewing the speed distribution towards low speed. This means that speed control via curve manipulation without altering the global average and standard deviation of train passing speed is feasible.

It was also noted that if an upper speed limit is enforced on a given site and corrugation control via speed variance increase is used, effects of widening the distribution may be cancelled out either partially or fully by the effect of having a high speed skew. In a worst case scenario, corrugation growth rate could increase as much as 34% under the chosen site simulation parameters. For this reason, speed distribution asymmetry effects should be considered before implementing a corrugation control system based on speed control.

REFERENCES

P.A. Bellette, P.A. Meehan, W.J.T. Daniel, 2008, "Effects of variable pass speed on wear-type corrugation growth", *Journal of Sound and Vibration* 314, pp. 616-634.

Daniel, W.J.T., Horwood, R.J., Meehan, P.A. and Wheatley, N., 2006, "Analysis of Rail Corrugation in Cornering", *Proc. Of 7th International Conference on Contact Mechanics and Wear of Rail/Wheel Systems (CM2006)*, Brisbane, Australia, September 24-26, 2006, pp. 159-166.

Grassie, S.L. and Cox, S.J., 1994, "The dynamic response of railway track with flexible sleepers to high frequency vertical excitation", *Proc Instn Mech Engrs* 198D No 7.

Hempelmann, K. and Knothe, K., 1996, "An extended linear model for the prediction of short pitch corrugation", *Wear* 191, pp. 161-169.

Hoffmannn, N.P. and Misol, M., 2007, "On the Role of Varying Normal Load and of Randomly Distributed Relative Velocities in the Wavelength Selection Process of Wear-Pattern Generation", *International Journal of Solids and Structures* 44, pp. 8718-8734.

Johnson, K.L., 1987, Contact Mechanics, Cambridge University Press, Cambridge.

Kampfer, B.O., 2006, "New approach for predicting wheel profile wear", *Proc. 7th International Conference on Contact Mechanics and Wear of Rail/Wheel Systems (CM2003)*, Brisbane, Australia, September 24-26, 2006, pp. 675-680.

Meehan, P.A., Bellette, P.A., Batten, R.D., Daniel, W.J.T., and Horwood, R.J., 2009, "A case study of wear-type rail corrugation prediction and control using speed variation", *Journal of Sound and Vibration* 325, pp. 85-105.

Polach, O., 2003, "Creep forces in simulations of traction vehicles running on adhesion limit", *Proc. 6th International Conference on Contact Mechanics and Wear of Rail/Wheel Systems (CM2003)*, Gothenburg, Sweden, 2003.

Sato, Y., Matsumoto, A. and Knothe, K., 2002, "Review on rail corrugation studies", *Wear* 253, pp. 130-139.

Shen, Z.Y., Hendrick, J.K. and Elkins, J.A., 1993 "A comparison of alternative creep force models for rail vehicle dynamic analysis", *Proc. 8th IAVSD Symposium*, Cambridge, MA, 1993.

APPENDICES

Appendix A - Nomenclature

b	half contact patch width (m)
B	creep equation exponent
C	track cant elevation (m)
$C_{\bar{\zeta}P}$	creep sensitivity given by equation 11
c_m	modal damping coefficient for mode, m (Ns/m)
d	lower domain limit of speed distribution (m/s)
e	speed distribution mode (m/s)
f	upper limit of speed distribution (m/s)
g	acceleration of gravity (m/s^2)
G	track gauge (m)
G_r	corrugation growth rate
h_b	height of bogie centre of mass from the rail (m)
h_{rc}	height of the geometric roll centre from the rail (m)
h_w	height of wagon centre of mass from the rail (m)
i	wheel number counted clockwise from front low
K_b	Wear sensitivity to contact deflection
$K_{b/eq}$	Equivalent single wheelpass wear for a bogie
k_c	rail head contact stiffness (N/m)
k_m	modal track stiffness for mode, m (N/m)
k_{roll}	rolling stiffness of the wagon at its roll centre
k_0	wear coefficient (see Kampfer, 2006)
L	length of bogie between wheels (m)
m	track mode number
m_b	mass of bogie per wheelset (kg)
m_m	modal track mass for mode, m (kg)
m_w	mass of wagon per wheelset (kg)
n	wheel pass number
p	probability density
ΔP	normal force variance (N)
P_H	normal force on high rail (N)
P_L	normal force on low rail (N)
Q	traction force (N)
r	corner radius (m)
R_m	modal track receptance for mode, m
R_{rv}	vertical receptance of the rail
R_{wv}	vertical receptance of the unsprung mass
S	standard skewness
v	train speed (m/s)
w_i	slip ratio
w_c	critical slip ratio
x	probability density scalar
y	yaw angle (rad)
Δz_0	steady state wear depth (m)
Z	profile height (m)
α	wagon roll (rad)
β	cant angle (rad)
θ	angle of attack at zero yaw (rad)
$\overline{x}$	average train passing speed (m/s)
μ_i	traction ratio for wheel i
μ_0	maximum coefficient of friction
μ_∞	coefficient of friction at infinite slip
ρ	density of rail steel (kg/m^2)
σ	speed standard deviation (m/s)
ω	frequency (rad/s)

Appendix B - Simulation parameters

Track properties

Corner radius (m)	300
Guage (m)	1.067
Cant elevation (m)	0.04

Train properties

Average speed (km/h)	60

Speed standard deviation (km/h)	12
Rolling stiffness (N.m/rad)	402000
Roll centre height (m)	0.25
Bogie centre height (m)	0.25
Wagon centre height (m)	1.6
Bogie mass (kg)	2271
Wagon mass (kg)	8218
Unsprung mass (kg)	970
Bogie length (m)	2.5
Contact properties	
Maximum coefficient of friction	0.4
High slip friction coefficient	0.3
Critican slip ratio	0.02
Creep curve exponent	0.02
Half contact patch width (m)	0.007
Wear coefficient	4×10^{-9}
Track material density (kg/m^3)	7800

Appendix C – Modal track model

The track receptance used in the simulations performed was created using a 5-mode theoretical model. Typically there are only two dominant modes in the frequency range at which corrugation grows (Grassie, 1994) so 5 modes are sufficient to overdetermine the system. The total track receptance as a function of frequency is given by the equation

$$R_{vr}(\omega) = \sum_{n=1}^{5} R_n(\omega),$$

where

$$R_n(\omega) = \frac{1}{k_m - m_m\omega^2 + i\omega c_m}.$$

The modal parameters used are given in the following table.

Mode	Mass, m (kg)	Stiffness, k (kN/m)	Damping, c (Ns/m)
1	380	162019	95504
2	40	2075046	400000
3	260	2739174	300000
4	100	1681623	26000
5	40	1021159	29000

Table 1. Track model modal parameters

The resultant absolute receptance given by these parameters is shown in Figure 12.

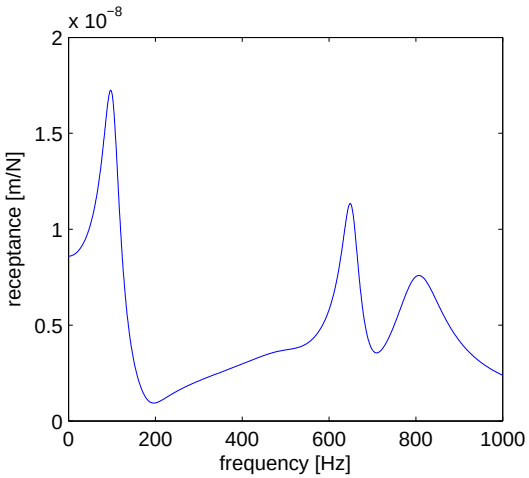

Figure 12. Theoretical modal rail receptance